Nanoscale

PAPER

View Article Online
View Journal | View Issue

Cite this: *Nanoscale*, 2015, **7**, 6151

Bio-inspired design of hierarchical PDMS microstructures with tunable adhesive superhydrophobicity†

Enshuang Zhang,[a] Youshan Wang,[d] Tong Lv,[a] Li Li,*[c] Zhongjun Cheng*[b] and Yuyan Liu*[a]

Received 17th January 2015,
Accepted 2nd March 2015

DOI: 10.1039/c5nr00356c

www.rsc.org/nanoscale

In this paper, bio-inspired PDMS films with different hierarchical microstructures were designed and tunable adhesive super-hydrophobicity was achieved on these films. The adhesive forces between a water droplet and the PDMS film can be adjusted from extremely low (about 8.3 μN) to very high (about 57 μN), and the tunable effect can be ascribed to different wetting states for the water droplets that result from different microstructures on the films. Noticeably, the obtained super-hydrophobic surfaces are acid/alkali-resisting, and water droplets with different pH values have similar contact angles and adhesive forces on the same surface. Finally, the application of the obtained surfaces for microdroplet transportation and self-cleaning are also discussed. The results reported herein provide a new method to obtain super-hydrophobic surfaces with controlled adhesion, and significantly improve our understanding of the relationship between surface adhesion, surface microstructures and the fabrication principle of tunable adhesive super-hydrophobic surfaces.

Introduction

In the past decade, super-hydrophobic surfaces have aroused much attention for their numerous applications,[1] for example self-cleaning,[2–9] anti-reflection,[10] microdroplet transportation,[11] oil–water separation[12,13] and bio-detection.[14] Surface adhesion is significant in determining the dynamic properties of a water droplet on the surface and ultimately affecting the application of the surface.[15] To meet the requirements of different applications, super-hydrophobic surfaces with controlled adhesion are desired, and thus it is important to develop a new method to design and process tunable adhesive surfaces.

Until now, a variety of efforts have been focused on such tunable adhesive super-hydrophobic surfaces.[16–52] Chen *et al.* fabricated silicon surfaces with periodic hydrophobic patterns (triangle, circle and rhombus) and superhydrophobic structures (dual-scale spikes induced by femtosecond laser). The tunable adhesion was achieved by adjusting the area ratio of the superhydrophobic domain to the hydrophobic domain.[18] Zhao *et al.* reported tunable adhesive polymeric surfaces with pillar structures by varying the aspect ratios.[22] Some other examples include the hydrothermal fabrication of MnO_2 films with ball cactus-like, mesh-like and titled nanorod structures,[36] the electro-deposition processing of TiO_2 with different pore structures,[26] dual-scale hierarchical anatase films,[37] as well as the electrochemical anodization for nanotubes,[38] and the thiol etching processing for fabricating $Cu(OH)_2$ with different morphologies.[31] Noticeably, all these have proven to be subject to certain limitations, such as severe processing conditions, high costs and poor durability. Meanwhile, although numerous nanostructures with various morphologies, as mentioned above, have been prepared to obtain tunable adhesive surfaces, the principle of microstructure design for such surfaces is still not very clear. Note that many plants leaves found in nature have super-hydrophobicity but different adhesions, which may innovate the design of special surface microstructures. For instance, lotus leaves, on which a water droplet can roll easily with a high contact angle (about 161°) and a low sliding angle (about 2°), are well known for their super-hydrophobic and self-cleaning abilities.[53,54] Rose petals are also super-hydrophobic[55] and a water droplet cannot

[a]*School of Chemical Engineering and Technology, Harbin Institute of Technology, Harbin, Heilongjiang 150001, P.R. China. E-mail: liuyy@hit.edu.cn; Fax: (+86)045186402368; Tel: (+86)045186413711*
[b]*Natural Science Research Center, Academy of Fundamental and Interdisciplinary Sciences, Harbin Institute of Technology, Harbin, Heilongjiang 150090, P.R. China. E-mail: chengzhongjun@iccas.ac.cn; Fax: (+86)045186412153; Tel: (+86)045186412153*
[c]*Department of Materials Science and Engineering, Cornell University, Ithaca, NY 14853, USA. E-mail: lilicmu@alumni.cmu.edu, lilicmu@gmail.com; Tel: +1-412-482-8712*
[d]*National Key Laboratory of Science and Technology on Advanced Composites in Special Environments, Harbin Institute of Technology, Harbin, Heilongjiang 150090, P.R. China*

†Electronic supplementary information (ESI) available: XRD of the templates; SEM image of porous Ni; Shapes of PDMS prepolymer on the template before and after heating; confocal microscopy images of the obtained templates; discussion of superhydrophobicity on the PDMS films. See DOI: 10.1039/c5nr00356c

roll and be pinned on their surface. Jiang *et al.* noted that different adhesions for water droplets on the above two leaves are due to the different morphologies and microstructure scales that result in different wetting states.[56] On lotus leaves, the water droplets reside in the lotus state (a special Cassie state with ultralow adhesion), and on rose petals the water droplet resides in the Cassie impregnating wetting state. These findings offer a new avenue for the design and preparation of super-hydrophobic surfaces with controlled adhesion, and it is reasonable to expect that tunable adhesive super-hydrophobic surfaces can be obtained by directly designing similar microstructures to those on lotus leaves and rose petals. However, the current correlated experimental research for the design of these microstructures is still rarely reported.

Polydimethylsiloxane (PDMS) is a type of stable, economic and biocompatible material, which has been widely used in the fabrication of super-hydrophobic surface for its intrinsic hydrophobicity. By introducing micro/nanostructures onto flat PDMS substrates, many kinds of super-hydrophobic PDMS have been reported.[57–61] Nevertheless, tunable adhesive super-hydrophobic PDMS surfaces are extremely rarely reported.[23,57] In this paper, inspired by lotus leaves and rose petals, we designed different microstructures with controllable adhesion on PDMS films by combining the electro-deposition and casting-replication techniques, and investigated the effect of surface microstructures on the surface adhesion. Briefly, Ni/NiO templates were firstly prepared through electro-deposition and post-annealing at different temperatures. Super-hydrophobic PDMS films with tunable water adhesion can be obtained after templated replication. The adhesive forces between the water droplet and PDMS film can be adjusted from extremely low (about 8.3 μN) to very high (about 57 μN). Meanwhile, the obtained surfaces have a particular acid/alkali-resisting ability, and water droplets with different pH values show similar wetting and adhesive performances on the same surfaces. Finally, their applications, such as micro-droplet transportation and self-cleaning of these surfaces, were also discussed. The current work provides us with a new strategy for the fabrication of super-hydrophobic surfaces with controlled adhesion, and greatly improves the understanding of the fabrication principle for tunable adhesive surfaces, which is essential for the future design of high performance super-hydrophobic surfaces with special advantages. To the best of our knowledge, this is the first report about the experimental preparation of tunable adhesive superhydrophobic surfaces based on the bio-inspired new design principle of directly imitating the microstructures of the lotus leaf and rose petal.

Experimental section

Materials

Nickel chloride ($NiCl{\cdot}6H_2O$, 98%) and ammonium chloride (NH_4Cl) were obtained from Tianjin chemical reagent factory, China. PDMS Sylgard 184 was purchased from Dow Corning, USA. Distilled water (>1.82 MΩ cm,) from the Milli-Q system was used.

Fabrication of super-hydrophobic PDMS films

The fabrication process of super-hydrophobic PDMS films is presented in Fig. 1, and can be divided into two steps: (1) fabrication of porous Ni/NiO templates with controlled microstructures,[61] and (2) templated replication with PDMS. Briefly, the porous templates were prepared through electro-deposition in a solution containing nickel chloride (0.2 M) and ammonium chloride (2 M). The processing procedure was conducted on an electrochemistry work station (KXN-6020D, Shenzhen Zhaoxin electronic instrument factory) at room temperature with a piece of stainless steel sheet (AISI 304, surface area ≈ 1 × 1 cm^2) as the cathode and a Pt plate as the counter electrode (anode, surface area = 1 ×1 cm^2). After electrodepositing for 30 seconds, the stainless steel with porous Ni was taken out, washed with deionized water and further dried with N_2. Finally, the obtained stainless steel sheets with porous Ni were annealed at different temperatures for 5 h in air to form the porous Ni/NiO templates with different microstructures. PDMS prepolymer was then poured into the as-prepared templates and cured in a conventional drying oven at 65 °C for about 12 h. Finally, the super-hydrophobic PDMS films with controlled microstructures and tunable adhesions can be obtained after careful peeling.

Characterization

The surface morphology was investigated with a field-emission scanning electron microscope (SEM) (HITACHI, SU8010). The water contact angles, sliding angles and advancing/receding

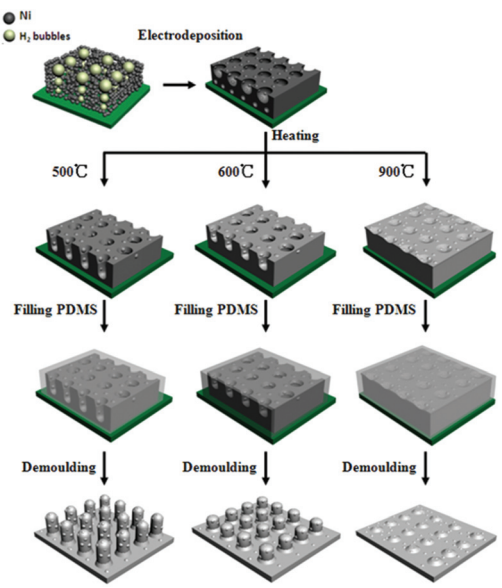

Fig. 1 Schematic illustration of the preparation process of super-hydrophobic PDMS films with controlled microstructures.

contact angles were examined on a contact angle measure meter (JC 2000D5, Shanghai Zhongchen Digital Technology Apparatus Co., Ltd) at ambient temperature. The contact angles were obtained by examining five different points on the same surface with a 4 μL water droplet and the average value was recorded. The sliding angles were then investigated five times for each surface by tilting the surface with a 4 μL water droplet on it until the droplet began to slide. The advancing and receding contact angles were obtained by increasing and decreasing the droplet volume on the surface, respectively. The acidic and basic water droplets were aqueous solutions containing hydrochloric acid and sodium hydroxide. The pH values of these droplets were measured by a pH meter (PB-10, Sartorius). All measurements of the adhesion forces for the super-hydrophobic surface were performed with a high-sensitivity microelectromechanical balance (Dataphysics DCAT 11, Germany). A water drop (4 μL) was first suspended with a metal cap, which was fixed to the balance, and the substrate was placed on the balance stage. The stage was moved upwards at a constant speed of 0.02 mm s^{-1}, until the surface contacted the droplet. The stage was then moved down, and the force increased gradually to maximum. When the surface broke away from the water droplet, the maximum force when the droplet is just leaving the surface was recorded as the adhesive force.

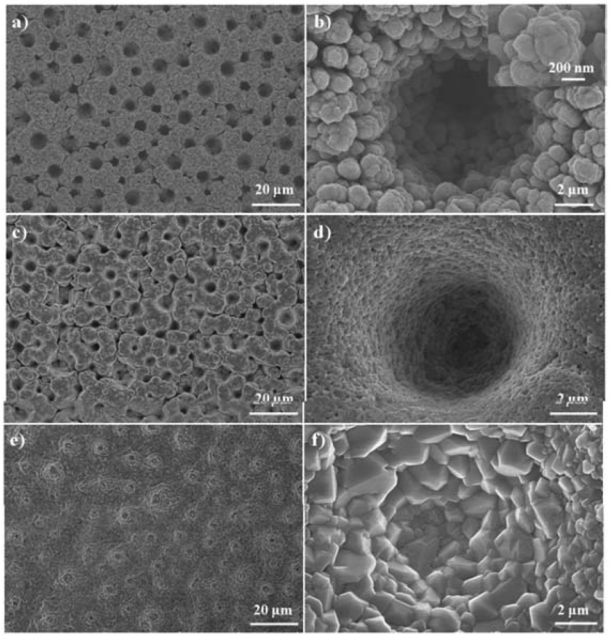

Fig. 2 SEM images of Ni/NiO microstructures obtained at different temperatures: (a) 500 °C, (c) 600 °C and (e) 900 °C. (b), (d) and (f) are higher magnification images corresponding to (a), (c) and (e), respectively. Inset in (b) is a further magnified image of the nanoparticles.

Results and discussion

By combining the electro-deposition process and post-annealing at different temperatures, different porous Ni/NiO microstructures can be obtained on stainless steel substrates (for more details see the ESI Fig. S1–S3†). Fig. 2 shows the SEM images of the microstructures obtained at different temperatures. On the surface obtained at about 500 °C, it can be observed that the surface shows a porous structure with typical pores of about 4–11 μm in diameter (Fig. 2a). The higher magnification image indicates that the surface of these pores is composed of numerous interconnected nanoparticle aggregates with a diameter of 1–3 μm (Fig. 2b), and the diameter of these nanoparticles are in the range of 100–300 nm (inset Fig. 2b). When the temperature increases to about 600 °C, the porous structure is still present (Fig. 2c). Nevertheless, the surface of these pores, as shown in Fig. 2d, becomes flatter compared with that shown in Fig. 2b. With the further increase of temperature to about 900 °C, it can be observed that the porous structure is no longer apparent (Fig. 2e). Meanwhile, some irregular blocks appear with sizes ranging from 1 μm to 2.5 μm. It is worth noting that as the temperature increases, the average depth of the pores seems to decrease (Fig. 2b, d and e). We then used confocal microscopy, one of the most powerful tools for material microstructure investigation,[62,63] to further accurately characterize the variation of pore depth (see the ESI Fig. S4†). As shown in Fig. S4,† the average depth decreases from about 8.6 μm to 4.7 μm with the increase of annealing temperature. The porous Ni/NiO template with different hierarchical microstructures can be obtained by simply controlling the annealing temperature.

The PDMS films with different microstructures were then templated by Ni/NiO after a simple replication process and the corresponding SEM images are shown in Fig. 3. For the film obtained on the Ni/NiO template prepared at 500 °C (Fig. 3a, the film is defined as S1), some pillars with a diameter range between 5 μm and 10 μm on the surfaces can be observed. The average height of the pillars is about 8.5 μm. Based on the higher magnification image (Fig. 3b), the pillar surfaces are not smooth and numerous pits can be seen on the pillars with the average diameter of 1.2 μm. In further magnifications, some folds with the width ranging from 50 nm to 150 nm can be detected on the pit surfaces (inset in Fig. 3b). For the film replicated on the template obtained at 600 °C (the film is defined as S2), the pillar structures still can be observed (Fig. 3c). Noticeably, the top surface of the pillars becomes smooth and the height of the pillars decreases to 7.4 μm (Fig. 3d). Fig. 3e shows the SEM image of the film obtained on the template annealed at 900 °C (the film is defined as S3) and it can be observed that the pillar structures disappear with many papillae dispersed on the surface. The average diameter and height of these papillae are about 15 μm and 4.6 μm (Fig. 3e), respectively. Some holes with the diameter of about 730 nm can be seen on these papillae (Fig. 3f). The microstructures on these PDMS films were further investigated by confocal microscopy and the results are consistent with the SEM results (see the ESI Fig. S5†). Both morphologies and microstructure scales in samples S1 and S3 are analogue to those of

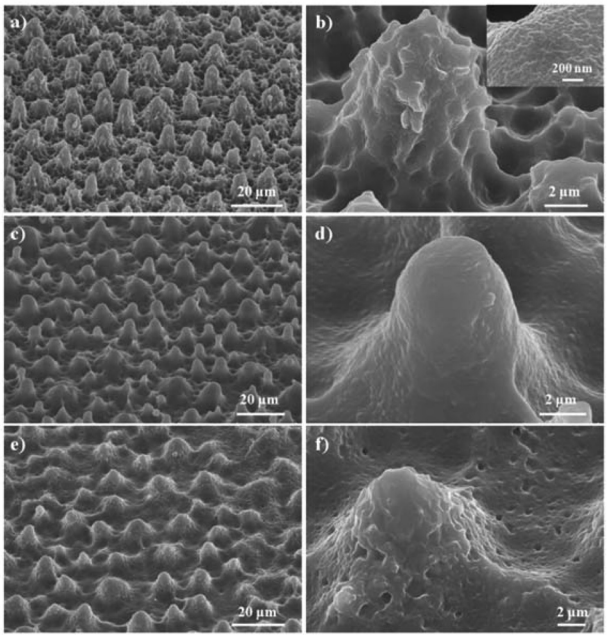

Fig. 3 SEM images of different PDMS films viewed at 45 degrees for different samples: (a) S1, (c) S2 and (e) S3. (b), (d), and (e) are the higher magnification images corresponding to (a), (c) and (e), respectively. Inset in (b) is a further magnified image of the pillar tip surface.

lotus leaves and rose petals, respectively.[54,56] These results indicate that by using Ni/NiO microstructures annealed at different temperatures as the templates, microstructures similar to those of plant leaves can be controlled on PDMS. It is expected that different wetting and adhesive performances can be observed on these films.

The wetting properties of the obtained PDMS films were examined on a contact angle measure meter. Fig. 4 shows the static and sliding contact angles of a water droplet (4 μL) on a flat PDMS film and the as-prepared PDMS films with different microstructures. On the flat PDMS film it can be seen that the surface is hydrophobic, highly adhesive and that a water droplet can be pinned with a contact angle of about 105°.[60] The other templated PDMS films show a remarkable change for both contact angle and sliding angle. As shown in Fig. 4, the water contact angles are all higher than 150° on the as-prepared samples (S1, S2 and S3), indicating that all these surfaces are super-hydrophobic. Such high hydrophobicity can be attributed to the enhanced effect of hierarchical micro/nanostructures on the intrinsic hydrophobicity of PDMS (for more discussion see the ESI†).[64,65]

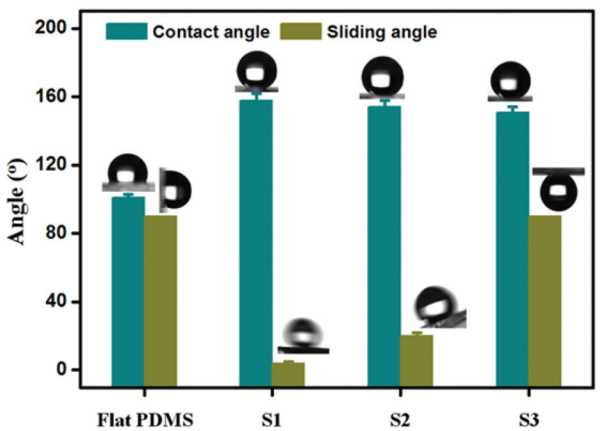

Fig. 4 Statistic results of contact angles and sliding angles on flat and hierarchical structured PDMS films, insets are the shapes of a water droplet on the related surface.

In this work, one of the major concerns is surface adhesion. Although all three as-prepared films have similar super-hydrophobicity, the dynamic actions of water droplets on these films are rather different (Fig. 4). A water droplet can roll easily with a sliding angle of about 3° for sample S1, indicating that the surface has low adhesion. For sample S2, the sliding angle is increased to about 20°, indicating the surface has an increased adhesion compared with S1. In the case of sample S3, a water droplet would be pinned firmly even when the film is turned upside down, demonstrating high adhesion on the surface. In addition to the sliding angle, the contact angle hysteresis for the three samples was also investigated. It is reported that different dynamic properties of water droplets are mainly attributed to different contact angle hysteresis.[66] As shown in Table 1, the contact angle hysteresis is different for the three as-prepared films with different microstructures. A surface with a low sliding angle has a small contact angle hysteresis, which is consistent with previous reports.[67]

As described above, the dynamic properties of water droplets on these surfaces as well as the surface adhesion are different for samples with different microstructures. By using a high-sensitivity microelectromechanical balance system, the adhesions of the as-prepared films were accurately investigated. Fig. 5 shows the force–distance curves recorded before and after the water droplet contacted the PDMS films. Firstly, the PDMS film was placed on the balance stage and a water droplet (4 μL) was suspended on a copper cap which was fixed on the balance system with the force of the system initialized to zero. The film was then moved upward at a rate of 0.02 mm s^{-1} to contact the water droplet while maintaining the force at zero (step 1 in the Fig. 5a). After contacting, the film was moved down and the balance force was increased to reach its maximum at the end of step 2. Finally, the film broke the water droplet away and the force decreased immediately (step 3). The maximum force when the droplet just leaves the film is defined as the adhesive force. Three lines with different

Table 1 The advancing/receding contact angles (θ_a/θ_r) and the contact angle hysteresis ($\Delta\theta = \theta_a - \theta_r$) for the as-prepared PDMS films

	S1	S2	S3
θ_a	159°	156°	152°
θ_r	157°	142°	105°
$\Delta\theta = \theta_a - \theta_r$	2°	14°	47°

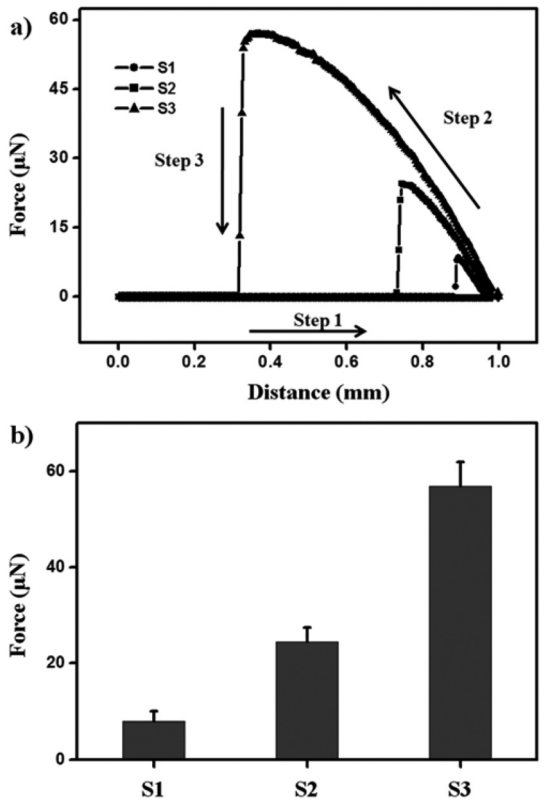

Fig. 5 (a) Force–distance curves for PDMS films with different microstructures. (b) Statistics of adhesive forces on the as-prepared PDMS films.

symbols represent the super-hydrophobic PDMS films with different the microstructures that show different adhesions, and the adhesive forces can be adjusted from extremely low (about 8 μN for S1) to very high (about 57 μN for S3) (Fig. 5b).

The mechanism affecting the adhesive force was carefully analyzed to understand the water-adhesion performances of those as-obtained PDMS films. As previously reported, surface adhesion is influenced by both the surface chemical composition and the microstructures.[15] In this work, the surface chemistry of the three films with the same chemical composition is similar and the surface microstructure would be the primary factor that influences surface adhesion. Surface adhesion (denoted as F) can be defined as a product of the liquid–solid interfacial interaction (denoted as I) and the contact area (denoted as A):[41]

$$F = kIA \quad (1)$$

$$F \propto A \quad (2)$$

where k is a constant and I is related to the solid surface chemistry and is supposed to be the same in this work for the PDMS films with the same chemical composition. Therefore, eqn (1) can be simplified to eqn (2), and surface adhesion is proportional to the contact area A. For sample S1, pillar-like structures with diameters between 5 μm and 10 μm disperse on the surface uniformly. Meanwhile, lots of folds with a diameter of 50–150 nm exist on these pillars. Interestingly, such hierarchical micro/nanostructures are similar to those on lotus leaves,[54] which show branch-like nanostructures with an average diameter of about 124.3 nm on the micropapillae in the diameter of 5–9 μm. A water droplet on such surfaces would reside in a special Cassie state, named lotus state (Fig. 6a).[68] In this state, a layer of air can be trapped among the hierarchical structures, which can prevent water from entering into the microstructures. Especially, the presence of nanostructures can lead to an extremely small solid–liquid contact area. Therefore, according to eqn (2), the surface has an extremely low adhesive force (Fig. 5) and a water droplet can roll easily on the surface with a low sliding angle (Fig. 4). In the case of sample S2, it can be observed that the pillar structures are still present and a water droplet would still reside in the Cassie state (Fig. 6b).[64,68] In this state, a layer of air trapped under the water droplet and the three-phase contact line is discrete and unstable, preventing water from intruding into the microstructures. Therefore, a water droplet can still roll on the surface. However, note that the top surface of the pillars on sample S2 become much smoother compared with sample S1, and the height of the pillars is also decreased. Hence, when a water droplet is placed on sample S2, it can wet

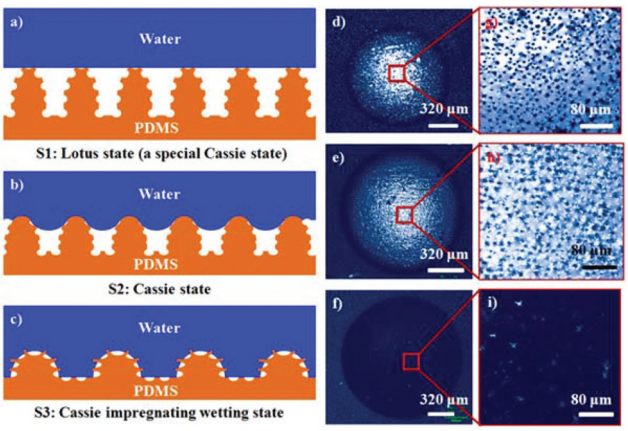

Fig. 6 Schematic illustration of the liquid–solid contact area: (a) for sample S1, lots of nanopits cover the micropillars, which can trap air among the hierarchical structures and result in an extremely low liquid–solid contact area, and thus, the water droplet would reside in the lotus state (a special Cassie state with an ultralow adhesion) and the surface shows super-hydrophobicity with extremely low adhesion; (b) for sample S2, pillar structures are still present and the water droplet resides in the Cassie state. However, the pillar tips become smooth and water can wet more solid surface area. Therefore, the liquid–solid contact area increased and the surface has an increased adhesion compared with S1; (c) for sample S3, large scale hierarchical micropapillae induce the water to reside in the Cassie impregnating wetting state. In this state, water can enter into the large gaps between micropapillae while maintaining the nanostructures dry, and thus the surface is super-hydrophobic as well as highly adhesive because of the large liquid–solid contact area; (d), (e) and (f) are the confocal microscopy images of samples S1, S2 and S3 under a water droplet, respectively; (g), (h) and (i) are the magnified images of (d), (e) and (f), respectively.

more solid surface and the liquid–solid contact area can increase. Such an increase can be further confirmed by the calculated results from the Cassie equation:[64]

$$\cos\theta_r = f_1 \cos\theta - f_2 \quad (3)$$

Herein, θ and θ_r are the contact angles for a water droplet on flat and rough PDMS surfaces, respectively. f_1 and f_2 are the fraction of solid and air under the droplet, respectively. In the current experiment θ is 105°, while θ_r are 158° and 154° for S1 and S2, respectively. According to eqn (3), the liquid–solid contact fraction for samples S1 and S2 are 0.098 and 0.137, respectively, indicating that sample S2 has a larger liquid–solid contact area than S1. According to eqn (2), sample S2 has a relatively high adhesive force (Fig. 5) and a higher sliding angle (Fig. 4) over sample S1. In the case of sample S3, the diameter of the papillae increases (the average diameter is about 15 μm) while the height further decreases (the average height is about 4.6 μm). Its similarity to sample S1 is that lots of pits (with an average diameter of about 730 nm) exist on these papillae. Noticeably, such microstructures are analogous to those on rose petals with nanoscale cuticular folds (with the diameter of about 700 nm) on the micropapillae (with the average diameter of about 16 μm).[55,56] On surfaces with such microstructures, a water droplet would reside in the Cassie impregnating wetting state (Fig. 6c).[56,68] In this state, water can enter into the large gaps between micropapillae (it is worth noting that water cannot wet the nanostructures on the micropapillae and the pit surface between the micropapillae, which is very important for the surface super-hydrophobicity), and a large contact area between water and solid film can be formed. According to eqn (2), a high adhesion would be produced and a water droplet can be pinned firmly even when the surface is turned upside down (Fig. 4). These illustrations can be further proved by the confocal microscopy results, as shown in Fig. 6d–i. In the case of samples S1 and S2, a lot of air can be trapped among the microstructures (the light blue areas in Fig. 6g and h represent the presence of air and dark blue areas are liquid–solid contact areas).[69] The amount of air is decreased obviously for sample S3, indicating that the contact area between the water droplet and surface is greatly increased. The result proves that sample S3 has the highest adhesion compared with S1 and S2, which is consistent with the dynamic contact angle results. Based on the results shown above, it can be found that the variation of surface morphology and microstructure scale can effectively lead to different adhesions on the super-hydrophobic surfaces.

The durability of the surface functional properties is very important for practical applications. In this work, the stability of the controllability on surface adhesion was also evaluated. The controllability remained for at least two months without special protection, indicating the excellent stability of the obtained surfaces. Moreover, the as-prepared surfaces exhibit a particular excellent acid/base-resisting ability. As shown in Fig. 7, no obvious fluctuation for both contact angles and adhesive forces is observed when the pH value of water varies between 1 and 14. To illustrate, the contact angles varied in the range of 155° and 159° with the increase of water pH for sample S1, and the adhesive forces changed between 7.5 μN and 10 μN. All of these results indicate that the obtained surfaces have a special acid/base-resisting ability and that water pH has little effect on super-hydrophobicity and surface adhesion.

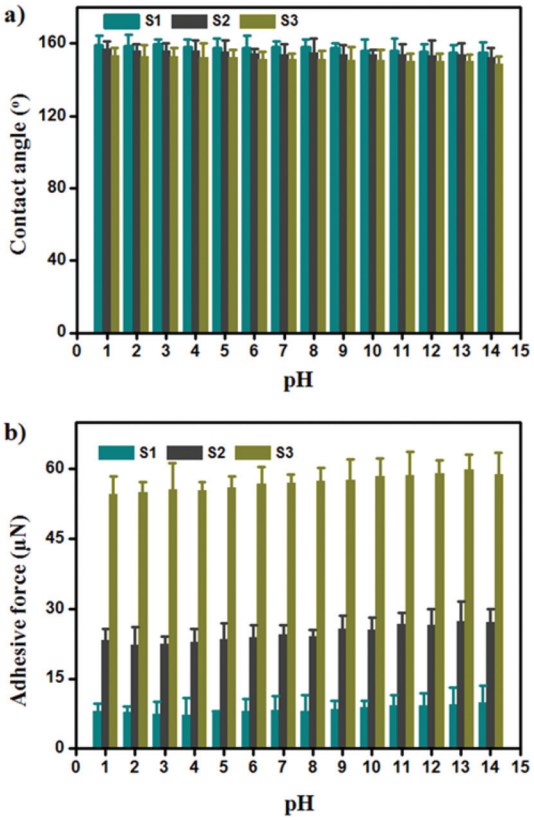

Fig. 7 Statistics of contact angles and adhesive forces for water droplets with different pH values on the as-prepared PDMS films, indicating that the obtained films have a special acid/basic-resisting property. Both values of contact angle and adhesive force are the average value from data in five different points on the same surface.

The super-hydrophobic PDMS films with regulated adhesion have many potential applications.[70,71] For example, the highly adhesive super-hydrophobic PDMS film can be used as a "mechanical hand" to realize the transportation of droplets with a certain weight from one surface to another.[72] As shown in Fig. 8, when a water droplet is placed on a low adhesive PDMS film, a highly adhesive PDMS film can touch and adhere the droplet, and then release the droplet onto a hydrophilic glass surface. No obvious loss and contamination of the droplet was observed during the whole process. This performance can endow the as-prepared highly adhesive PDMS film with more applications, such as bio-detection and microsample analysis.

Similarly to the lotus leaf, the low adhesive super-hydrophobic PDMS film can be used as a self-cleaning surface, and the motion of water droplets can remove dust from the surface.[73] As shown in Fig. 9a, a low adhesive super-hydro-

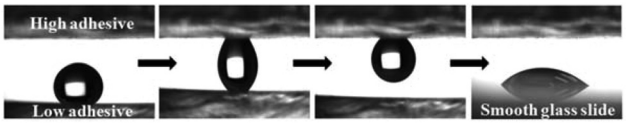

Fig. 8 Process of droplet transportation using the highly adhesive super-hydrophobic PDMS film as a "mechanical hand".

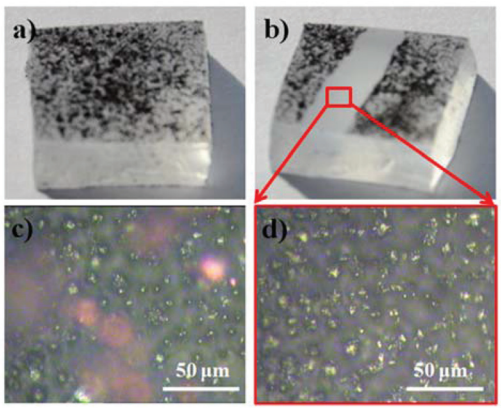

Fig. 9 Optical photos of a super-hydrophobic PDMS low adhesive surface before (a) and after partial washing (b) by water droplets, respectively. (c) and (d) optical microscopy images corresponding to the PDMS surfaces before and after washing by water droplets, respectively. (Pink spots correspond to the methylene blue particles).

phobic PDMS film was deliberately contaminated by some methylene blue. Some water droplets were then dropped onto the surface to examine their surface self-cleaning ability. It can be noticed that on the surface where the water droplets have passed, the methylene blue was removed easily and a clean surface was left (see the corresponding movie in the ESI†). Fig. 9c and d show the optical microscopy images of the surface before and after washing with droplets, respectively. No methylene blue can be seen on the surface, further confirming the excellent self-cleaning ability of the obtained low adhesive super-hydrophobic PDMS films.

Conclusions

To conclude, a series of bio-inspired super-hydrophobic PDMS films with tunable adhesions were designed with similar hierarchical microstructures to those on lotus leaves and rose petals. The adhesive forces between the films and water droplet can be controlled from extremely low (about 8 μN) to very high (about 57 μN). The tunable effect is ascribed to the transition from lotus state to the Cassie impregnating wetting states for a water droplet, which results from the different morphologies and microstructure scales on the films. Meanwhile, the as-prepared films have a special acid/basic-resisting ability and water droplets with different pH values have similar wetting and adhesive performances on the same surface. Based on the special tunable adhesive property, the applications of these films on droplet transportation and self-cleaning for high and low adhesive surfaces were developed, respectively. The results reported herein are important for enhancing the understanding of the influence of surface microstructure on surface adhesion and the fabrication principle for tunable adhesive super-hydrophobic surfaces. Furthermore, their simple processing and controllable water adhesion extend the applications of materials shown in the current work to wide applications, such as microfluidic devices, droplet-based microreactors and bio-detection.

Acknowledgements

This work is supported by the National Natural Science Foundation of China (NSFC grant no. 21304025), the Fundamental Research Funds for the Central Universities (grant no. HIT. KISTP.201408), the Research Fund for the Doctoral Program of Higher Education of China (20112302120062) and the Heilong Jiang Postdoctoral Funds for scientific research initiation (LBH-Q13063).

Notes and references

1 X. Yao, Y. Song and L. Jiang, *Adv. Mater.*, 2011, **23**, 719.
2 X. M. Li, D. Reinhoudt and M. Crego-Calama, *Chem. Soc. Rev.*, 2007, **36**, 1350.
3 R. Blossey, *Nat. Mater.*, 2003, **2**, 301.
4 A. Lafuma and D. Quéré, *Nat. Mater.*, 2003, **2**, 457.
5 P. Roach, N. J. Shirtcliffe and M. I. Newton, *Soft Matter*, 2008, **4**, 224.
6 M. J. Hancock, K. Sekeroglu and M. C. Demirel, *Adv. Funct. Mater.*, 2012, **22**, 2223.
7 X. Zhang, F. Shi, J. Niu, Y. Jiang and Z. Wang, *J. Mater. Chem.*, 2008, **18**, 621.
8 V. A. Ganesh, H. K. Raut, A. S. Nair and S. Ramakrishna, *J. Mater. Chem.*, 2011, **21**, 16304.
9 X. Liu, Y. Liang, F. Zhou and W. Liu, *Soft Matter*, 2012, **8**, 2070.
10 W. L. Min, B. Jiang and P. Jiang, *Adv. Mater.*, 2008, **20**, 3914.
11 X. Hong, X. F. Gao and L. Jiang, *J. Am. Chem. Soc.*, 2007, **129**, 1478.
12 J. K. Yuan, X. G. Liu, O. Akbulut, J. Q. Hu, S. L. Suib, J. Kong and F. Stellacci, *Nat. Nanotechnol.*, 2008, **3**, 332.
13 M. Jin, J. Wang, X. Yao, M. Liao, Y. Zhao and L. Jiang, *Adv. Mater.*, 2011, **23**, 2861.
14 W. Song, D. D. Veiga, C. A. Custódio and J. F. Mano, *Adv. Mater.*, 2009, **21**, 1.
15 M. Liu, Y. Zheng, J. Zhai and L. Jiang, *Acc. Chem. Res.*, 2010, **43**, 368.
16 Z. Hu, X. Zhang, Z. Liu, K. Huo, P. K. Chu, J. Zhai and L. Jiang, *Adv. Funct. Mater.*, 2014, **24**, 6381.

17 D. Wu, S. Wu, Q. Chen, Y. Zhang, J. Yao, X. Yao, L. Niu, J. Wang, L. Jiang and H. Sun, *Adv. Mater.*, 2011, **23**, 545.
18 D. Zhang, F. Chen, Q. Yang, J. Yong, H. Bian, Y. Ou, J. Si, X. Meng and X. Hou, *ACS Appl. Mater. Interfaces*, 2012, **4**, 4905.
19 L. Heng, X. Meng, B. Wang and L. Jiang, *Langmuir*, 2013, **29**, 9491.
20 B. Bhushan, *Langmuir*, 2012, **28**, 1698.
21 J. B. K. Law, A. M. H. Ng, A. Y. He and H. Y. Low, *Langmuir*, 2014, **30**, 325.
22 H. Shahsavan, D. Arunbabu and B. Zhao, *Macromol. Mater. Eng.*, 2012, **297**, 743.
23 J. Yong, F. Chen, Q. Yang, D. Zhang, H. Bian, G. Du, J. Si, X. Meng and X. Hou, *Langmuir*, 2013, **29**, 3274.
24 J. Pu, S. Wan, Z. Lu, G. Zhang, L. Wang, X. Zhang and Q. Xue, *J. Mater. Chem. A*, 2013, **1**, 1254.
25 S. N. Ramakrishna, L. Y. Clasohm, A. Rao and N. D. Spencer, *Langmuir*, 2011, **27**, 9972.
26 Y. Lai, X. Gao, H. Zhuang, J. Huang, C. Lin and L. Jiang, *Adv. Mater.*, 2009, **21**, 3799.
27 W. Zhao, L. Wang and Q. Xue, *J. Phys. Chem. C*, 2010, **114**, 11509.
28 J. Li, X. Liu, Y. Ye, H. Zhou and J. Chen, *J. Phys. Chem. C*, 2011, **115**, 4726.
29 B. Bhushan and E. K. Her, *Langmuir*, 2010, **26**, 8207.
30 M. Toma, G. Loget and R. M. Corn, *ACS Appl. Mater. Interfaces*, 2014, **6**, 11110.
31 Z. Cheng, M. Du, H. Lai, N. Zhang and K. Sun, *Nanoscale*, 2013, **5**, 2776.
32 T. Darmanin and F. Guittard, *Soft Matter*, 2013, **9**, 1500.
33 Z. Yang, F. Chien, C. Kuo, D. Chueh and P. Chen, *Nanoscale*, 2013, **5**, 1018.
34 M. K. Dawood, H. Zheng, T. H. Liew, K. C. Leong, Y. L. Foo, R. Rajagopalan, S. A. Khan and W. K. Choi, *Langmuir*, 2011, **27**, 4126.
35 W. Lee, B. G. Park, D. H. Kim, D. J. Ahn, Y. Park, S. H. Lee and K. B. Lee, *Langmuir*, 2010, **26**, 1412.
36 X. D. Zhao, H. M. Fan, X. Y. Liu, H. Pan and H. Y. Xu, *Langmuir*, 2011, **27**, 3224.
37 J. Huang, Y. Lai, L. Wang, S. Li, M. Ge, K. Zhang, H. Fuchs and L. Chi, *J. Mater. Chem. A*, 2014, **2**, 18531.
38 Z. Hu, X. Zhang, Z. Liu, K. Huo, P. K. Chu, J. Zhai and L. Jiang, *Adv. Funct. Mater.*, 2014, **24**, 6381.
39 A. Milionis, D. Fragouli, L. Martiradonna, G. C. Anyfantis, P. D. Cozzoli, I. S. Bayer and A. Athanassiou, *ACS Appl. Mater. Interfaces*, 2014, **6**, 1036.
40 M. Wolfs, T. Darmanin and F. Guittard, *Soft Matter*, 2012, **8**, 9110.
41 J. Ou, W. Hu, C. Li, Y. Wang, M. Xue, F. Wang and W. Li, *ACS Appl. Mater. Interfaces*, 2012, **4**, 5737.
42 T. Pisuchpen, N. Chaim-ngoen, N. Intasanta, P. Supaphol and V. P. Hoven, *Langmuir*, 2011, **27**, 3654.
43 C. Wang, T. Wang, C. Liao, S. Kuo and H. Lin, *J. Phys. Chem. C*, 2011, **115**, 16495.
44 Z. Guo, X. Chen, J. Li, J. Liu and X. Huang, *Langmuir*, 2011, **27**, 6193.
45 H. Teisala, M. Tuominen, M. Aromaa, M. Stepien, J. M. Mäkelä, J. J. Saarinen, M. Toivakka and J. Kuusipalo, *Langmuir*, 2012, **28**, 3138.
46 D. Ishii, H. Yabu and M. Shimomura, *Chem. Mater.*, 2009, **21**, 1799.
47 Y. Wu, Y. Xue, X. Pei, M. Cai, H. Duan, W. T. S. Huck, F. Zhou and Q. Xue, *J. Phys. Chem. C*, 2014, **118**, 2564.
48 L. Taajamaa, E. Kontturi, J. Lainea and O. J. Rojas, *J. Mater. Chem.*, 2012, **22**, 12072.
49 B. Balu, V. Breedveld and D. W. Hess, *Langmuir*, 2008, **24**, 4785.
50 Y. Lai, C. J. Lin, J. Y. Huang, H. F. Zhuang, L. Sun and T. Nguyen, *Langmuir*, 2008, **24**, 3867.
51 R. D. Mundo, F. Palumbo and R. d'Agostino, *Langmuir*, 2008, **24**, 5044.
52 M. Wang, C. Chen, J. Maab and J. Xu, *J. Mater. Chem.*, 2011, **21**, 6962.
53 W. Barthlott and C. Neinhuis, *Planta*, 1997, **202**, 1.
54 L. Feng, S. Li, Y. Li, H. Li, L. Zhang, J. Zhai, Y. Song, B. Liu, L. Jiang and D. B. Zhu, *Adv. Mater.*, 2002, **14**, 1857.
55 B. Bhushan and E. K. Her, *Langmuir*, 2010, **26**, 8207.
56 L. Feng, Y. Zhang, J. Xi, Y. Zhu, N. Wang, F. Xia and L. Jiang, *Langmuir*, 2008, **24**, 4114.
57 X. Huang, D. Kim, M. Im, J. Lee, J. Yoon and Y. Choi, *Small*, 2009, **5**, 90.
58 J. Genzer and K. Efimenko, *Science*, 2000, **290**, 2130.
59 M. H. Jin, X. J. Feng, J. M. Xi, J. Zhai, K. Cho, L. Feng and L. Jiang, *Macromol. Rapid Commun.*, 2005, **26**, 1805.
60 M. H. Sun, C. X. Luo, L. P. Xu, H. Ji, Q. Ouyang, D. P. Yu and Y. Chen, *Langmuir*, 2005, **21**, 8978.
61 K. Cheng, D. Cao, F. Yang, D. Zhang, P. Yan, J. Yin and G. Wang, *J. Power Sources*, 2013, **242**, 141.
62 Q. Yuan and Y. Zhao, *J. Fluid Mech.*, 2013, **716**, 171.
63 Q. Yuan, X. Huang and Y. Zhao, *Phys. Fluids*, 2014, **26**, 092104.
64 A. B. D. Cassie and S. Baxter, *Trans. Faraday Soc.*, 1944, **40**, 546.
65 R. N. Wenzel, *Ind. Eng. Chem.*, 1936, **28**, 988.
66 M. Y. Yüce, A. L. Demirel and F. Menzel, *Langmuir*, 2005, **21**, 5073.
67 Z. Cheng, R. Hou, Y. Du, H. Lai, K. Fu, N. Zhang and K. Sun, *ACS Appl. Mater. Interfaces*, 2013, **5**, 8753.
68 S. Wang and L. Jiang, *Adv. Mater.*, 2007, **19**, 3423.
69 J. Gao, Y. Yao, Y. Zhao and L. Jiang, *Small*, 2013, **9**, 2515.
70 G. Gong, K. Gao, J. Wu, N. Sun, C. Zhou, Y. Zhao and L. Jiang, *J. Mater. Chem. A*, 2015, **3**, 713.
71 G. Gong, J. Wu, Y. Zhao, J. Liu, J. Xu and L. Jiang, *Soft Matter*, 2014, **10**, 549.
72 M. Jin, J. Wang, X. Yao, M. Liao, Y. Zhao and L. Jiang, *Adv. Mater.*, 2011, **23**, 2861.
73 D. Nyström, J. Lindqvist, E. stmark, P. Antoni, A. Carlmark, A. Hult and E. Malmström, *ACS Appl. Mater. Interfaces*, 2009, **1**, 816.

